Bearing Strength of Pin-Connected Polymer Composites Subjected to Dynamic Loading

Taner Yilmaz, Tamer Sinmazcelik
Kocaeli University, Mechanical Engineering Department, Engineering Faculty, Veziroglu Campus, Izmit 41040, Turkey

In this study, static load bearing strength of pin-connected carbon fiber-reinforced polyphenylenesulphide (PPS) composites that have $[(0^\circ/90^\circ)]_{3s}$ stacking sequence was investigated. Firstly, the samples were loaded dynamically, and then the same samples were loaded statically. The results obtained from this sequential experiment were compared with the results obtained from samples that were loaded only statically. In addition, the fatigue life and failure mechanisms were investigated with respect to the selection of the geometrical parameters. Dynamic and static loading experiments were performed according to the ASTM STP 749 and ASTM D953 standards, respectively. To obtain optimum load bearing values, the ratio of distance between the edge and hole center to hole diameter (*E*/*D*) and ratio of sample width to hole diameter (*W*/*D*) has been systematically changed. According to the experimental results, maximum load bearing values have been obtained when *E*/*D* ratio was equal to 2. POLYM. COMPOS., 31:25–31, 2010. © 2009 Society of Plastics Engineers

INTRODUCTION

Carbon fiber reinforced plastic (CFRP) laminates are widely used in engineering structures. They serve under a wide range of temperature values and different environments. Furthermore, because many structures are subjected to cyclic or variable loading conditions, information about fatigue strength is particularly important. CFRPs are used under high or low cyclic loadings, because of that, the behavior of CFRPs should be well known and investigated [1].

Mechanical fatigue is the most common failure mode of structures in service, both for homogeneous and composite materials. The relative importance of fatigue has yet to be reflected in design, where static conditions still prevail [2].

Most of the previous fatigue experiments on mechanically fastened composite joints have been done at room temperature, whereas little work has been done at elevated temperatures. At room temperature, Garbo et al. [3] found that the fatigue failure modes and the critical geometries to ensure bearing failure in fatigue are similar to those observed for static loading. In tension–tension fatigue of pin loaded CFRPs, Herrington and Sabbaghian [4] found stress levels below 70% of ultimate static strength.

Xioxou et al. [5] have investigated experimental fatigue life of cross-ply graphite/epoxy composite laminates having $[0^\circ/90^\circ_2]_s$, $[0^\circ_2/90^\circ_2]_s$, and $[0^\circ_2/90^\circ_4]_s$ stacking sequences.

Mandell and Meier [6] note that fatigue failure in general is characterized by the progressive accumulation of cracks in the matrix and at the fiber/matrix interface, resulting in loss of strength and stiffness.

Fatigue behavior of composite bolted joints has been investigated experimentally, in which the fatigue life and damages were examined with respect to the design parameters of the joints and environmental effects. Crews [7] studied the static and fatigue behavior of joints with respect to bolt clamping force and environmental effects. Liu et al. [8] found that the fatigue life decreased as the environmental temperature and humidity increased. Herrington and Sabbaghian [4] studied the effects of applied stress levels, orientation of the outer layer, reinforcing filaments, and the bolt torque level on the fatigue life of a graphite-epoxy composite. They have used the $W/D = 4$ and $E/D = 4$ geometric configuration. They found the endurance limit of the joint as about 67% of the plate's bearing strength. From a study on the static and fatigue performance of adhesive/bolted hybrid joints, Fu and Mallick [9] reported that the hybrid joints have higher static failure load capacity and longer fatigue life than the adhesive joints.

In the present study, an experimental investigation has been carried out to investigate the static load bearing capacity of pin connected carbon/polyphenylenesulphide (PPS) composites with $[(0^\circ/90^\circ)]_{3s}$ stacking sequence that were firstly loaded (1,000 cycles) dynamically. The ratio of the edge distance to the pin diameter (E/D), and the ratio of the specimen width to the pin diameter (W/D) were

Correspondence to: T. Yilmaz; e-mail: taneryilmaz2002@yahoo.com
DOI 10.1002/pc.20843
Published online in Wiley InterScience (www.interscience.wiley.com).

TABLE 1. Geometry of the joints and pins.

L (mm)	*W* (mm)	*D* (mm)	*W/D*	*E/D*
40, 45, 55, 65, 75, 95	20, 40	5, 10	2, 4, 8	1, 2, 4, 6

systematically varied during experiments. This study highlights the effects of cyclic loading on the strength and fatigue performance of a carbon/PPS composite system. In particular, it addresses the change in tension-tension ($R = 0.1$) fatigue behavior of pin connected carbon/PPS composite.

EXPERIMENTAL METHOD AND MATERIAL

In this study, continuous carbon fiber reinforced PPS matrix composite laminates with $[(0^\circ/90^\circ)]_{3s}$ lay-up were used. Materials were obtained from Ten Cate (Nijverdal/Holland) as hot pressed laminates in dimensions of 450 × 450 × 2 mm. The volume fraction of the fibers was 51%. The laminates were composed of a total of six layers, and a unit layer thickness of 0.31 mm. Unit weight of each layer was 479 g/m^2. Commercial code of the laminates was CF0286.

The samples were prepared according to the geometrical parameters shown in Table 1. For every single parameter, at least eight samples have been tested and the average of the values was taken into account.

Dynamic loading tests were conducted with reference to ASTM STP 749 at room temperature of (20°C under the load control function of a DARTEC servohydraulic testing machine that has 60 kN loading capacity [7]. The load control function of the machine assured that a constant maximum and constant minimum alternating loads were applied to the specimen during the experiment. The loading waveform was sinusoidal with frequency of 1 Hz. Sample geometry and tensile test setup used during the dynamic loading are shown in Fig. 1. The applied varying stress is defined by the components σ_{max} and R, where R is $\sigma_{min}/\sigma_{max}$. In this investigation, the stress ratio used for all fatigue tests was $R = 0.1$.

In the calculations, we have considered a σ_o/σ_{br} ratio which does not cause more than 0.04 D elongation in the pin hole after 1,000 cycles. In this equation, σ_o is the applied maximum stress, and σ_{br} is the bearing strength. From our previous experiments [10–13], the bearing strength of the materials under static loading conditions for different geometrical parameters is already known. We have chosen the fatigue endurance limit as 60% ($\sigma_o = 0.6\ \sigma_{br}$) of these known bearing strength values. After the fatigue test was initiated, it was performed until the desired number of cycles (1,000 cycles) was achieved.

Static loading performance of dynamically loaded samples was investigated according to ASTM D953 standard at 20°C [14, 15]. Experiments were done with Instron 4411 that has a computer controlled 5 kN loading capacity. The static loading tests were carried out with displacement control at a rate of 1 mm/min.

EXPERIMENTAL RESULTS AND DISCUSSION

As it is seen in Fig. 2, composite samples that are firstly dynamically loaded (FDL) show smaller bearing strength values compared to samples which are only statically loaded (SL). From the results obtained of our previous studies [10–13], the optimum parameters are known as: $W/D = 2$, $E/D = 2$, and $D = 10$ mm. This situation is valid for either dynamically and SL or only SL samples. Minimum load bearing values for FDL samples are seen to be the same for the geometric parameters that are used in only static loading. These geometric parameters were $W/D = 8$, $E/D = 1$, and $D = 5$. When Fig. 2 is carefully observed, it can be seen that the maximum load bearing values are obtained when $E/D = 2$. As the E/D value is increased, there is not a dramatic change in the results. Because of that the critical E/D ratio in $[(0^\circ/90^\circ)]_{3s}$ lay-up is 2.

In Fig. 3, load-displacement curves for only SL and FDL pin connected samples were presented. The load bearing capacity and energy storage observed until fracture for only SL pin-connected samples is higher when compared with FDL samples. This situation is valid for all of the geometric parameters. In addition, as the W/D ratio for both types of test samples were increased, the load bearing values of the samples decreased.

The load-displacement curves for $D = 10$ mm samples are shown in Fig. 4. The reduction in the bearing strength of the samples, which were tested under fatigue loading, is due to various failure mechanisms. Composites, due to their anisotropic structure, show very complicated failure mechanisms. For most of the materials, crack formation is

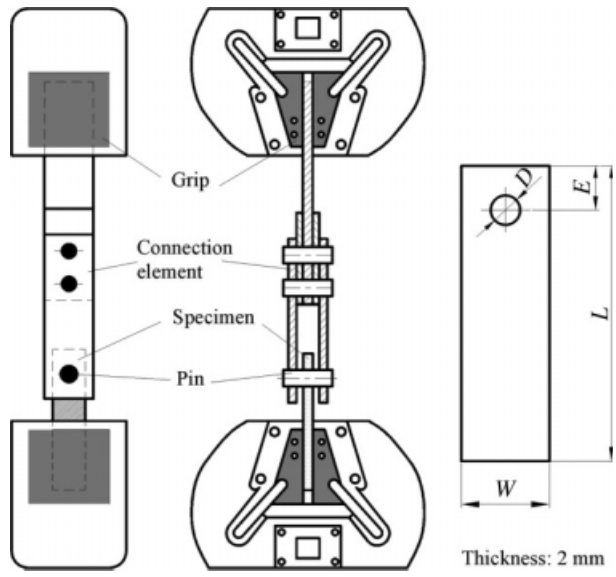

FIG. 1. Schematic illustration of the test setup for the fatigue tests of the composite pin joint.

DOI 10.1002/pc

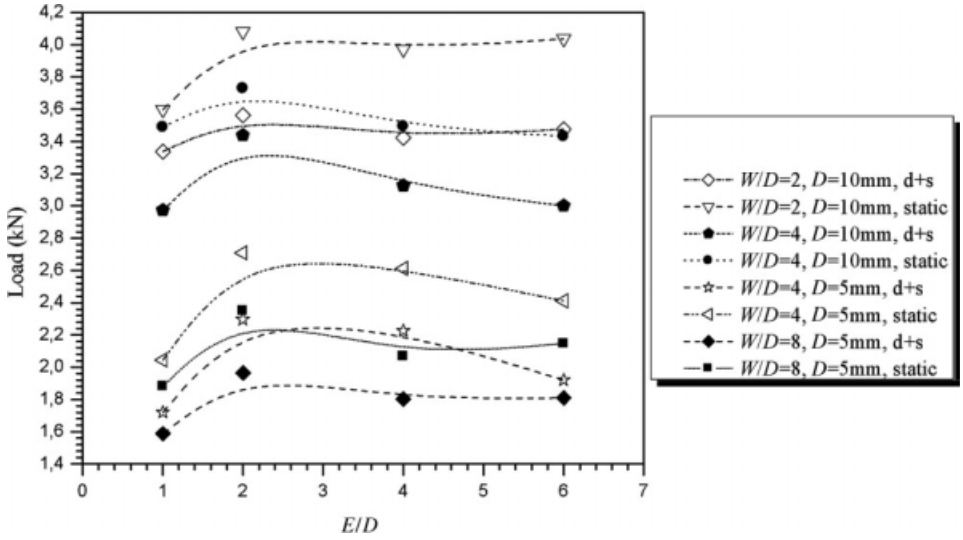

FIG. 2. Variation of the ultimate load values with respect to *E/D* ratio in only statically and both dynamically and SL samples.

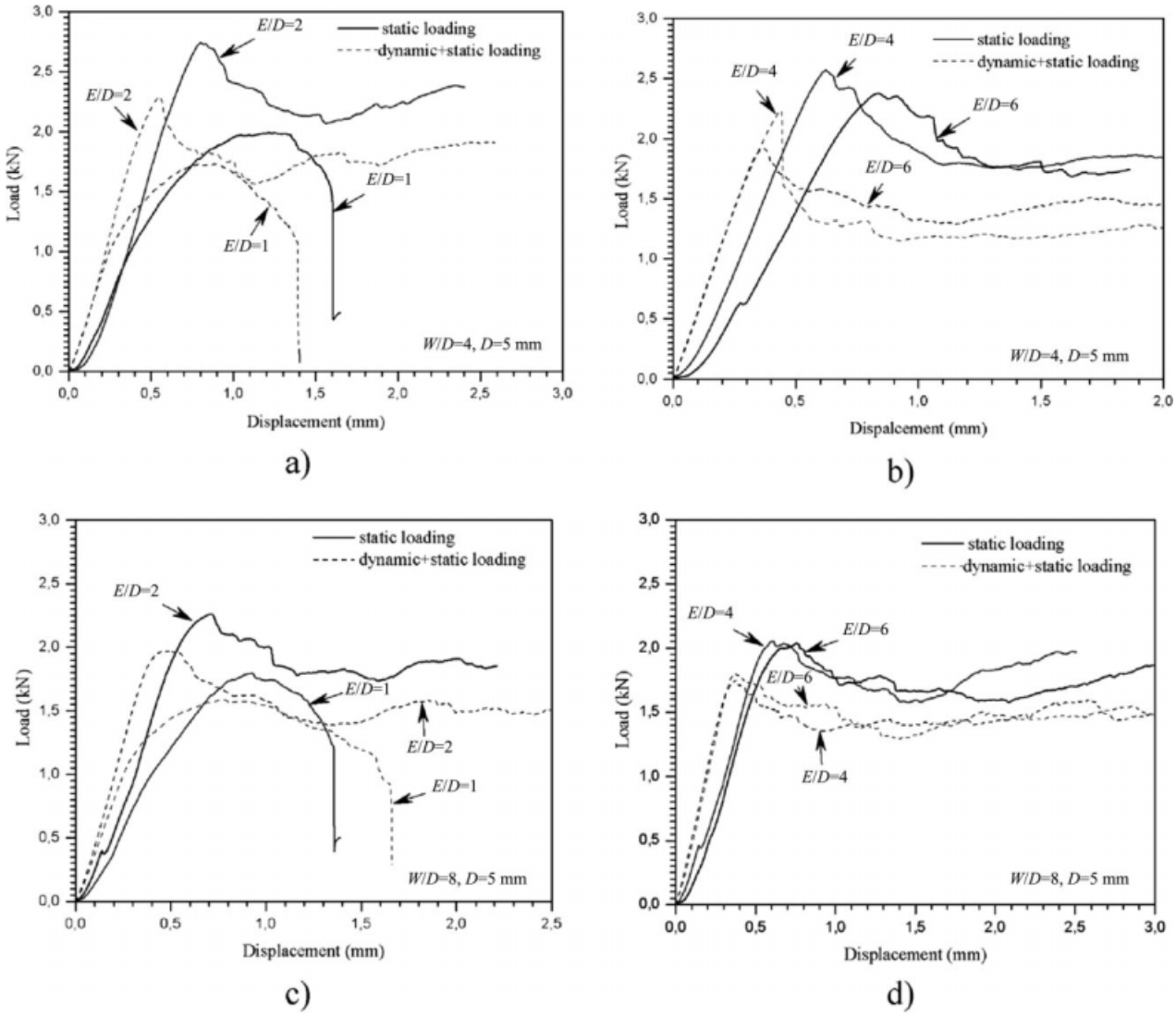

FIG. 3. Load-displacement curves for only statically loaded and firstly dynamically loaded samples ($W/D = 4$, $W/D = 8$, $D = 5$ mm).

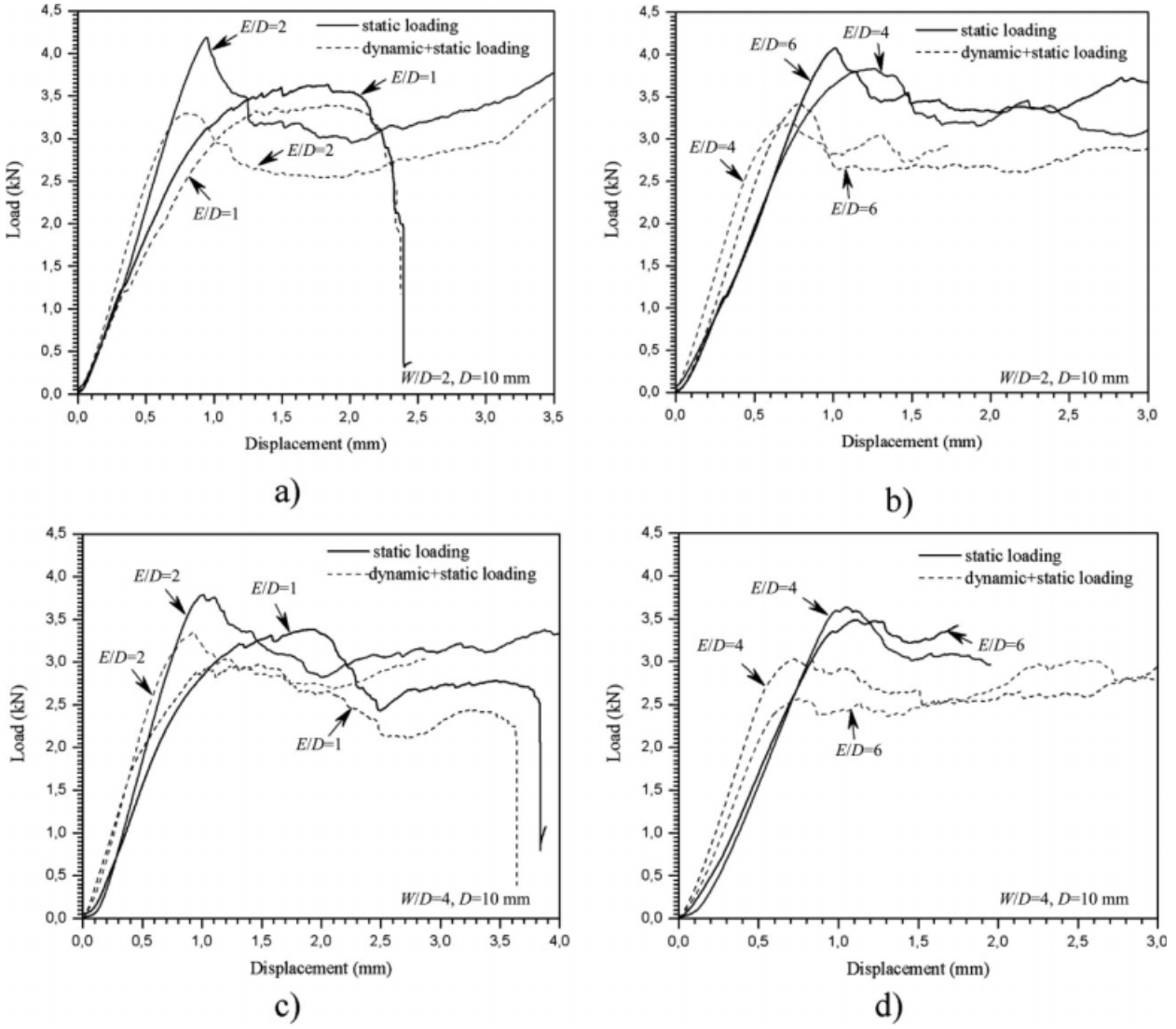

FIG. 4. Load-displacement curves for only statically loaded and firstly dynamically loaded samples ($W/D = 2$, $W/D = 4$, $D = 10$ mm).

the main fatigue loading failure mechanism. However, in composites there are different failure mechanisms due to fatigue loading. These mechanisms are crack formation in the matrix, fiber fracture, delamination, and fiber/matrix debonding. These fatigue loading failures are the factors that reduce the strength and the rigidity of composite materials.

As it is seen from both Figs. 3 and 4, the failure mechanism of the samples exposed to dynamic loading did not change. However, the load bearing capacity of the test

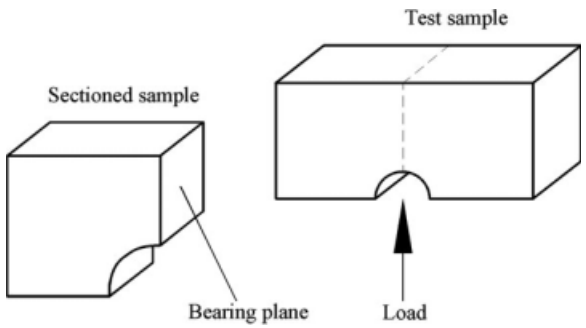

FIG. 5. Sample sectioning for determination of the bearing plane.

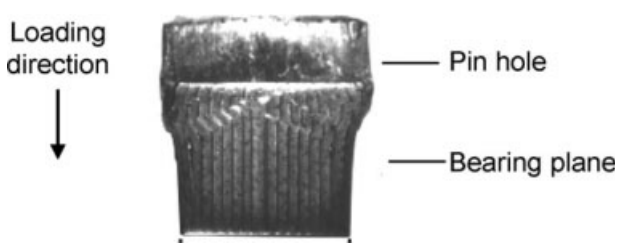

FIG. 6. Photograph of the bearing plane [16].

 DOI 10.1002/pc

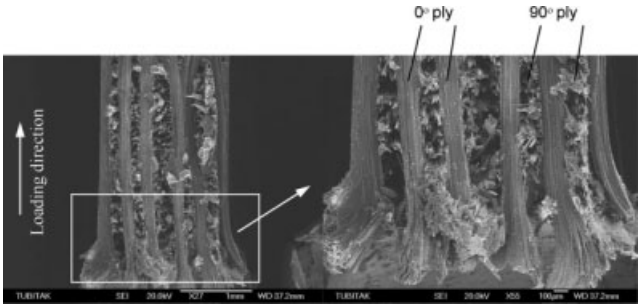

FIG. 7. The deformation types observed on the bearing plane at the edge of the pin hole.

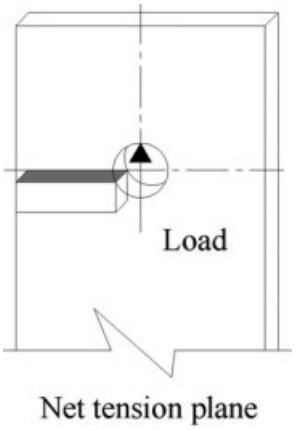

FIG. 8. The plane at which net tension failure is observed.

samples reduced due to the formation of various failure mechanisms (matrix cracking, fiber-matrix debonding, etc.) during the dynamic loading. From Figs. 3 and 4, it is seen that the failure mode in the connection region is bearing. As a conclusion, it is possible to say that the failure mechanisms are effective at the bearing plane of the samples.

To understand the bearing failure mode in the samples, the cross-sections from the maximum load bearing region, in other words from the bearing plane of the samples, were taken (see Fig. 5). The micrograph showing this cross-section is illustrated in Fig. 6. Delaminations between 0° oriented laminates, buckling, and fracture of the fibers are the observed failure mechanisms in the end of the dynamic loading test. Delaminations between laminates cause interlaminar discontinuities. Delaminated laminates are exposed to compressive forces. These forces cause instabilities and buckling of the fibers in the laminates. As the number and the length of delaminated layers increase, structures reach their critical buckling strength limit and the laminates are buckled. As a result of this phenomenon, samples show bearing failure mode [16].

Deformations at the sample edges are shown in Fig. 7. There might be two reasons for the deformations at the sample edges. The first one is bending of the pin and the second one is related with edge effects. The first reason, which is bending of the pin, is caused because of the load transferred at the pins. During the load transfer, the pin is elastically bent upwards and caused deformations at the edges. This phenomenon increases the stress at the edges and causes excessive deformation at the outer region of the pin hole. The second reason, which is the edge effects, can be explained as follows: outer layers of the composite materials are not well supported as the layer in the middle part of the composite material. Hence, the failure sensitivity of the outer layers is higher compared to the central layers. As a result, edges are more severely deformed compared to the middle layers of the composite materials. The deformation types observed at the edges of the samples show similarities with deformation types published in previous studies [10–13]. These studies have shown that the cracks and crushes are the fundamental types of mechanisms in the formation of bearing failure mode [17]. As a conclusion, delaminations, buckling, and fracture of the fibers are the reasons for the deformation of the FDL samples (see Fig. 7).

Different from bearing failure mode, some of the FDL and SL samples showed bearing+net tension failure mode depending on the sample geometry. The mechanisms that were related with net tension failure mode and located at the tension plane (see Fig. 8) were explained below.

The tension plane is the plane which is responsible for the determination of the fatigue life of carbon fiber reinforced PPS composites with $(0^\circ_n/90^\circ_m)_s$ stacking sequence. After the first application of the load, there will be a multitude in the distribution of fiber breaks in the volume of the material. Debonding initiate from the distributed fiber breaks. As debonding grows, the stress profiles in neighboring fibers continually change and weak parts fail because of the stress distribution.

Because of the elastic property difference between fiber and matrix, debonding around fibers propagate, unite, and form macroscopic scale cracks in the direction perpendicular to the loading. These cracks propagate in the direction perpendicular to the loading and become the reason for the final failure. To clearly understand the fail-

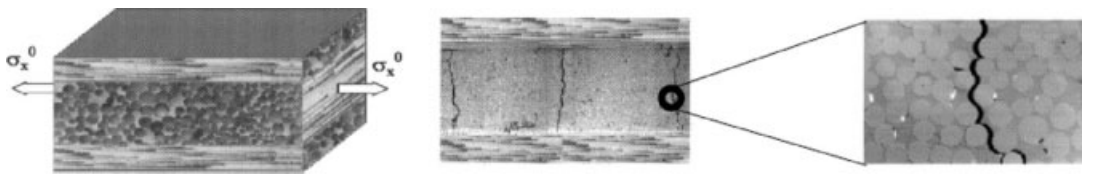

FIG. 9. Formation of cracks in transverse plies from coalescence of fiber-matrix debonds [18].

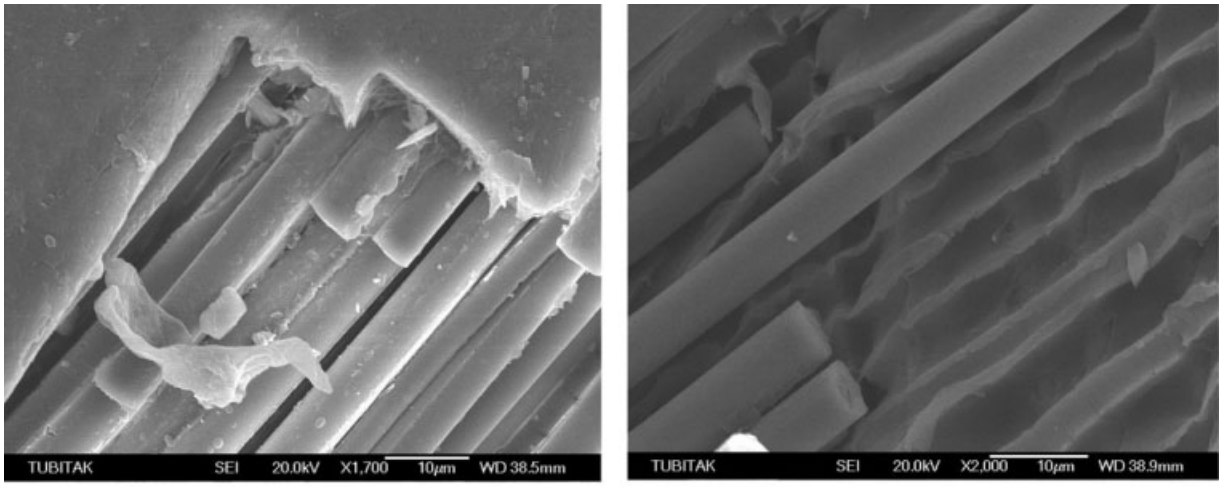

FIG. 10. Fractographic scanning electron micrographs for (a) only statically loaded and (b) firstly dynamically loaded samples.

ure mechanism explained above, it is important to observe the failure evolution at the $(0^{\circ}_{n}/90^{\circ}_{m})_{s}$ lay-ups. The tensile stress concentrations at the critical plies parallel to the loading axis affect the failure formation and local degradation of samples. In Fig. 9, the transverse crack formation in 90° ply is shown.

Scanning electron micrographs of fibers at the fracture surface of failed specimens are shown in Fig. 10. There were differences in the fracture surfaces of carbon-fiber/PPS composites subjected to fatigue and static tensile tests. The surface of carbon-fiber/PPS specimens which failed because of static tensile tests were rougher in appearance, when compared with those that failed under dynamic loading. This fractographic difference is another indication that debonding is a prevalent fatigue mechanism in carbon-fiber/PPS composites. Comparing failure surfaces of the two specimens, FDL samples showed notably more sprawling and uneven fractures when compared with only SL samples.

The ultimate load capacities of pin loaded samples are presented in Fig. 11. To find the optimum geometry for the joints, *E*/*D* and *W*/*D* ratios were systematically varied during the experiments. The specimens have different width (*W*), pin hole diameter (*D*), *E*/*D*, and *W*/*D* values. It is seen from the curves that FDL samples give lower ultimate load values compared to only SL specimens.

In this experimental study, it is concluded that the cracks due to fatigue loading initiated at the fiber/matrix interface, where components with different elastic properties meet. Microscopic separations between the fiber and

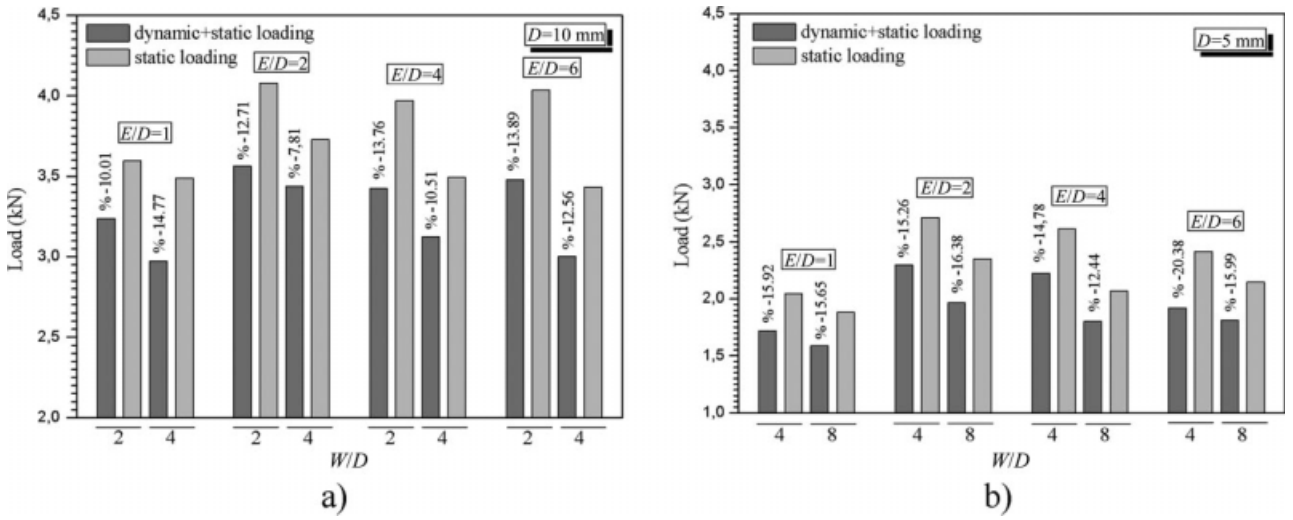

FIG. 11. Ultimate failure loads versus *W*/*D* ratio.

 DOI 10.1002/pc

the matrix are the clues of this conclusion. Debonding in the fiber/matrix interface causes serious problems especially during the dynamic loading of the composite materials. These small microscopic separations become larger and larger as the dynamic loading continues and eventually final failure occurs due to the growth of the microscopic separations.

With the failure mechanisms discussed above, the drop in the ultimate bearing failure load values of the samples exposed to dynamic loading was tried to be explained. For the joints that will be exposed to the loading types explained above, it is important to consider the possible failure mechanisms and select the design parameters according to that.

CONCLUSIONS

In this study, pinned-joint experiments have been performed to examine both dynamic (1,000 cycles) and static strength behavior on a carbon/PPS laminate with $[(0^\circ/90^\circ)]_{3s}$ stacking sequences. The drop in the bearing strength after dynamic loading is explained with the fracture of the fibers and fiber/matrix debonding due to internal structural failure. Debonding formed at fiber/matrix interface can be defined as the most important failure mechanism that is responsible for the reduction in the performance of the joints. To obtain the optimum geometry, the ratio of the edge distance to the pin diameter (E/D), and the ratio of the specimen width to the pin diameter (W/D) have systematically been varied during the tests. After the investigation of all the geometrical parameters, it is concluded that the samples exposed to both dynamic (1,000 cycles) and static loading with $E/D = 2$, $W/D = 2$, and $D = 10$ mm show the maximum bearing strength. $[(0^\circ/90^\circ)]_{3s}$ joints reach their bearing strength limit at those ratios. After the dynamic loading, ultimate bearing failure load values reduce down to $\sim$13% of the static strength while ratios are $E/D = 2$, $W/D = 2$, and $D = 10$ mm. However, the samples that are only exposed to static loading give higher endurance limit compared to FDL samples.

REFERENCES

1. Y. Nakai and C. Hiwa, *Int. J. Fatigue*, **24**, 161 (2002).
2. E. Kristofer Gamstedt, L.A. Berglund, and T. Peijs, *Compos. Sci. Technol.* **59**, 759 (1999).
3. S.P. Garbo, J.M. Ogonowski, and H.E. Reiling. "Effect of Variances and Manufacturing Tolerances on the Design Strength and Life of Mechanically Fastened Composite Joints, Vols. **1 & 2**, AFWALTR-81-3041," Air Force Wright Aeronautical Laboratory, Dayton (OH), April (1981).
4. P.D. Herrington and M. Sabbaghian, *J. Compos. Mat.*, **27**, 491 (1993).
5. D. Xioxou, B. Larry, and M. Shokrieh, *Compos. Sci. Technol.*, **59**, 2025 (1999).
6. J.F. Mandell and U. Meier, "Effects of Stress Ratio, Frequency, Loading Time on Tensile Fatigue of Glass-Reinforced Epoxy," In *Long-Term Behavior of Composites*, T.K. O'Brien, Ed., American Society for Testing and Materials, Philadelphia (PA), 55 (1983).
7. J.H. Crews Jr., "Bolt-Bearing Fatigue of a Graphite/Epoxy Laminate," In *Joining of Composite Materials*, K.T. Kedward, Ed., ASTM STP 749, Philadelphia, PA, 131 (1981).
8. D. Liu, W.G. Gau, K.D. Zhang, and B.Z. Ying, *Theor. Appl. Fract. Mech.*, **19**, 145 (1993).
9. M. Fu and P.K. Mallick, *Int. J. Adhesion Adhesive*, **21**, 145 (2001).
10. T. Yılmaz and T. Sınmazcelik, *Mater. Des.*, **28**, 520 (2007).
11. T. Yılmaz and T. Sınmazcelik, *Mater. Des.*, **28**, 1695 (2007).
12. T. Yilmaz and T. Sinmazcelik, *Polym. Compos.*, DOI 10.1002/pc. 20771 (2008).
13. T. Yilmaz and T. Sinmazcelik, *Polym. Compos.*, DOI 10.1002/pc. 20808 (2008).
14. ASTM D 953-D, *Standard Test Method for Bearing Strength of Plastics*, ASTM Designation, Philadelphia, PA, 342.
15. A. Aktaş, *Compos. Struct.*, **67**, 485 (2005).
16. W.A. Counts and W.S. Johnson, *Int. J. Fatigue*, **24**, 197 (2002).
17. P.P. Camanho, S. Bowron, and F.L. Matthews, *J. Reinf. Plast. Compos.*, **17**, 205 (1998).
18. K.E. Gamstedt, *J. Appl. Polym. Sci.*, **76**, 457 (2000b).